Organic Electronics 33 (2016) 213–220

Contents lists available at ScienceDirect

Organic Electronics

journal homepage: www.elsevier.com/locate/orgel

Two-dimensional conjugated copolymers composed of diketopyrrolopyrrole, thiophene, and thiophene with side chains for binary and ternary polymer solar cells

Wan-Chien Li [a], You-Ren Liu [a], Jhe-Han Chen [b], Wei-Che Chang [b], Pai-Tao Sah [b], Li-Hsin Chan [b, *]

[a] Department of Applied Chemistry, National Chi Nan University, Nantou, 54561, Taiwan, ROC
[b] Department of Applied Materials and Optoelectronic Engineering, National Chi Nan University, Nantou, 54561, Taiwan, ROC

ARTICLE INFO

Article history:
Received 16 December 2015
Received in revised form
8 March 2016
Accepted 16 March 2016
Available online 26 March 2016

Keywords:
Two-dimensional conjugated copolymer
Diketopyrrolopyrrole
Thiophene with side chains
Ternary polymer solar cell

ABSTRACT

Two new two-dimensional conjugated copolymers (named *r*-**PTTDPP50** and *r*-**PTTDPP75)** consisting of a diketopyrrolopyrrole (DPP) derivative, thiophene with a conjugated side chain, and 2,5-bis(trimethylstannyl)thiophene were designed and synthesized via Stille cross-coupling reactions for use in bulk heterojunction (BHJ) polymer solar cells (PSCs); the feed-in ratios were varied to obtain the copolymers. It was found that the content of DPP units in the copolymer main chain significantly affected the molecular weight, absorption range, electronic energy level, and morphology of thin films of the copolymers. In the thin-film state, both copolymers exhibited a broad absorption band with two obvious peaks and a vibronic shoulder, as well as an absorption edge for wavelengths of up to 1000 nm. The vibronic shoulder in the absorption spectrum of *r*-**PTTDPP75** was more intense than that in the spectrum of *r*-**PTTDPP50,** owing to the presence of a greater number of coplanar DPP units in the former. Electrochemical measurements indicated that the highest occupied molecular orbital (HOMO) energy levels for *r*-**PTTDPP50** and *r*-**PTTDPP75** were −5.16 and −5.19 eV, respectively, while their lowest unoccupied molecular orbital (LUMO) energy levels were −3.89 and −3.99 eV, respectively. On increasing the number of electron-deficient DPP segments in *r*-**PTTDPP75**, the LUMO energy level was lowered. Further, its HOMO energy level was also affected. BHJ PSCs composed of the electron-donor copolymers blended with an electron acceptor, namely [6,6],-phenyl-C61-butyric acid methyl ester ($PC_{61}BM$) or [6,6]-phenyl-C71-butyric acid methyl ester ($PC_{71}BM$), in 1:2 wt ratio were fabricated and characterized. The power conversion efficiency (PCE) of the *r*-**PTTDPP50**/$PC_{71}BM$-based (w/w = 1:2) PSC reached 2.32% for an open-circuit voltage of 0.632 V, short-circuit current of 9.81 mA/cm^2, and fill factor of 37.4%, under the illumination of AM 1.5G (100 mW/cm^2). Ternary blend BHJ solar cells formed by doping *r*-**PTTDPP50** into the common binary blend of P3HT and $PC_{61}BM$ were also investigated. The optimized *r*-**PTTDPP50**:P3HT:$PC_{61}BM$ device exhibited a PCE of 3.85%, which was significantly higher than that of the P3HT:$PC_{61}BM$ device (2.97%).

1. Introduction

Bulk heterojunction (BHJ) polymer solar cells (PSCs) prepared using a conjugated polymer as an electron donor and a fullerene derivative (e.g. [6,6],-phenyl C_{61} butyric acid methyl ester ($PC_{61}BM$) or [6,6]-phenyl C_{71} butyric acid methyl ester ($PC_{71}BM$)) as an electron acceptor have been studied extensively over the past two decades [1–3]. Their power conversion efficiencies (PCEs) have been increased to more than 10% [4–6]. A large number of conjugated polymers have been developed to improve the photovoltaic properties of BHJ PSCs. Further, various design strategies have been proposed to increase the PCEs of such cells. In order to fabricate PSCs with a high PCE, the conjugated polymer used must satisfy the following important criteria: (i) they must exhibit a broad absorption band, so that the short-circuit current (J_{sc}) is high; (ii) their lowest unoccupied molecular orbital (LUMO) energy level must be appropriately offset from that of the acceptor; (iii) they must have a

* Corresponding author.
E-mail address: lhchan@ncnu.edu.tw (L.-H. Chan).

http://dx.doi.org/10.1016/j.orgel.2016.03.018
1566-1199/

low-lying highest occupied molecular orbital (HOMO); (iv) they must exhibit a nanoscale interpenetrating network-like morphology, so that the interfacial area is high and efficient charge separation and transport can be realized; and (v) they must show high charge carrier mobilities, so that both charge collection and J_{sc} are high, because of the resulting decrease in the rate of charge recombination [7–11].

Of the various strategies proposed for designing semiconducting polymers, a particularly effective one is to combine electron-rich and electron-deficient units to form a donor-acceptor (D-A) system. This strategy has been used widely to obtain systems with a low bandgap. Further, the HOMO and LUMO energy levels of such a system can be adjusted through appropriate molecular design. However, most polymers have an absorption range of 350–650 nm along with a wide bandgap (E_g) (greater than 1.6 eV); because of which the full solar spectrum cannot be used [12,13]. Near-infrared (NIR) materials, which can absorb radiation with wavelengths of 650–1000 nm, are crucial for organic photovoltaic devices. Therefore, it is highly desirable to develop rapid and concise design strategies for assembling a diversity-oriented library of π–conjugated polymers that can be used to screen the NIR polymers [14]. Diketopyrrolopyrrole (DPP)-containing polymers have attracted much attention and are considered potential NIR materials, because they exhibit a broad absorption spectrum covering the visible and NIR regions and have attractive optoelectronic properties. BHJ PSCs and organic field effect transistors based on DPP-contain polymers exhibit improved performance [15–23].

Two-dimensional (2D) conjugated polymers have attracted much attention as high-performance conjugated donor materials for use in PSCs; because of their conjugated side groups or side chains, which broaden the absorption spectrum of the polymers, as well as their high hole mobility and their relatively low HOMO energy levels [24–30]. Moreover, recent studies on ternary blend solar cells, which are a novel concept, have shown that such cells can easily extend the absorption spectral range and improve the photon-harvesting ability, thus improving device performance [31–34]. Ternary blend BHJ PSCs consist of two donors and one acceptor (or one donor and two acceptors). The main advantage of this configuration is the simpler sandwich-like architecture and easier fabrication, compared to the tandem cell configuration. A number of studies have investigated P3HT/$PC_{61}BM$ or $PC_{71}BM$ systems while using small molecules or polymers as organic additives to form ternary blend solar cells. The criteria for selecting the appropriate organic additives for blending into the ternary P3HT/$PC_{61}BM$ or $PC_{71}BM$ systems are that the additive should have appropriate offset energy levels with respect to P3HT and $PC_{61}BM$ or $PC_{71}BM$ and have a complementary absorption range with respect to P3HT. The performance of ternary BHJ PSCs can be improved by optimizing the doping concentration of the organic additive used [35]. In this study, based on the above considerations, two 2D conjugated D-A copolymers (named ***r*-PTTDPP50 and *r*-PTTDPP75**) that contained DPP, thiophene with a conjugated side chain, and 2,5-bis(trimethylstannyl)thiophene (this was accomplished by varying the feed-in ratios) were designed and synthesized via Stille cross-coupling reactions for use in BHJ PSCs. To synthesize the copolymers, the DPP derivative was employed as an electron-withdrawing unit while thiophene with a side chain and 2,5-bis(trimethylstannyl)thiophene were used as the electron-donating units. The resulting copolymers exhibited electron D-A architectures, 2D configurations, and wide absorption bands. The effects of the feed-in ratios of the monomers on their photophysical, electrochemical, and photovoltaic properties were investigated in detail. The morphological and photovoltaic characteristics of films of the copolymer/fullerene derivative blends are discussed. In addition, owing to the complementary absorption properties of P3HT, ternary blend PSCs based on P3HT:$PC_{61}BM$ and containing ***r*-PTTDPP50** in different weight ratios were also investigated. This work shows that the number of DPP units in the copolymer main chain significantly affects the molecular weight, absorption range, electronic energy level, and morphology of the resulting thin films. Further, the copolymers synthesized in this study have potential for use as secondary sensitizers in ternary blend PSCs.

2. Experimental

2.1. Materials

All the chemicals used were obtained either from Aldrich, Alfa Aesar, or TCI Chemical Co., and were used as received unless noted otherwise. All solvents, including diethyl ether, dichloromethane, ethyl acetate, chlorobenzene, *o*-dichlorobenzene (*o*-DCB), tetrahydrofuran (THF), *N*,*N*-dimethylformamide (DMF), and toluene, were freshly distilled and dried over appropriate drying agents prior to use. 2,5-bis(2-ethylhexyl)-3,6-bis[5-bromothiophene-2-yl]-2,5-dihydropyrrolo[3,4-*c*]pyrrole-1,4-dione (**DPPBr**) [36] was synthesized according to a previously reported method. (*E*)-4-(5-(2-(2,5-dibromothiophen-3-yl)vinyl)thiophen-2-yl)-*N*,*N*-diphenylaniline (**MTD**) was synthesized in the laboratory using a previously established procedure [37–39]. 2,5-Bis(trimethylstannyl) thiophene and tetrakis(triphenylphosphine)palladium were obtained from Sigma-Aldrich Chemical Company. $PC_{61}BM$, $PC_{71}BM$, and poly(3,4-ethylenedioxythiophene):poly(styrenesulfonate) (PEDOT:PSS) were purchased from Lumtec and H. C. Starck, and used as received.

2.2. *Synthesis of r-PTTDPP50*

A mixture of **MTD** (594 mg, 1.0 mmol), 2,5-bis(trimethylstannyl) thiophene (820 mg, 2.0 mmol), and **DPPBr** (683 mg, 1.0 mmol) was dissolved in 30 mL of anhydrous toluene. The reaction mixture was purged with N_2 and subjected to three freeze-pump-thaw cycles to remove O_2. Next, $Pd(PPh_3)_4$ (46.2 mg, 4.0 mol% with respect to the ditin monomer) was added to the reaction mixture, and the reaction was allowed to proceed at 85–90 °C for at least 48 h. Subsequently, the mixture was cooled to room temperature, and then poured into a solution (400 mL) of methanol and deionized water (3:1). A fibrous precipitate was obtained by filtration. The precipitate was then dissolved in chloroform and reprecipitated in methanol. Further purification was performed by Soxhlet extractions using acetone, ethyl acetate, and tetrahydrofuran. The resulting polymer, ***r*-PTTDPP50**, was obtained as a black solid in an isolated yield of 45% after drying under vacuum for 24 h. Gel permeation chromatography (GPC) tetrahydrofuran (THF): Weight-average molecular weight (M_w) = 203.2 kg/mol and polydispersity index (PDI, M_w/M_n) = 1.18. ^{1}H Nuclear Magnetic Resonance (NMR) spectrum (CD_2Cl_2, 300 MHz, δ/ppm): 9.12–8.81 (br, thiophene-H), 7.70–6.72 (m, Ph-H and thiophene-H), 4.18–3.70 (br, *N*-CH_2), 2.11–0.55 (m, alkyl-H).

2.3. *Synthesis of r-PTTDPP75*

***r*-PTTDPP75** was synthesized using **MTD** (297 mg, 0.5 mmol), 2,5-bis(trimethylstannyl) thiophene (820 mg, 2.0 mmol), **DPPBr** (1.02 g, 1.5 mmol), and $Pd(PPh_3)_4$ (46.2 mg, 4.0 mol% with respect to the ditin monomer) by the method described above for ***r*-PTTDPP50**. The resulting polymer was obtained as a deep-black solid in 55% yield after drying under vacuum for 24 h. GPC (THF): Weight-average molecular weight (M_w) = 358.2 kg/mol and polydispersity index (PDI, M_w/M_n) = 1.10. ^{1}H NMR ($CDCl_3$, 300 MHz, δ/

ppm): 9.20–8.80 (br, thiophene-H), 7.30–6.72 (m, Ph-H and thiophene-H), 4.18–3.81 (br, *N*-CH_2), 2.12–0.63 (m, alkyl-H).

2.4. Characterization of copolymers

General. The ^{1}H NMR spectra were recorded on a Varian Unity Inova 300WB NMR spectrometer at room temperature. The molecular weights of the copolymers were determined using GPC, which was performed on a Waters GPC-1515 system with a refractive index detector (2414); THF was used as the eluent and polystyrene as the standard. The thermal decomposition temperatures (T_d) of the copolymers were determined by thermogravimetric analysis (TGA), which was performed using a Perkin-Elmer TGA-7 analyzer at a scanning rate of 10 °C/min between 30 and 800 °C in an atmosphere of nitrogen. The ultraviolet–visible (UV–vis) absorption spectra were recorded using a Hewlett-Packard 8453 spectrophotometer. The redox potentials of the polymers were determined by cyclic voltammetry (CV), which was performed using an electrochemical analyzer (CHI 612D; scanning rate of 50 mV s^{-1}) equipped with Pt electrodes. A Ag/Ag^+ (0.10 M $AgNO_3$ in MeCN) electrode was used as the reference electrode, while the electrolyte was an anhydrous N_2-saturated solution of 0.1 M Bu_4NClO_4 in MeCN. A Pt plate coated with a thin polymer film was used as the working electrode, while the counter and reference electrodes were a Pt wire and a Ag/Ag^+ electrode, respectively. The electrochemical potential was calibrated against ferrocene/ferrocene$^+$. The surface morphologies of the polymer thin films were characterized in the tapping mode with an atomic force microscopy (AFM) system (SII SPA400, Seiko Instruments Inc.), operated under an ambient atmosphere.

2.5. Fabrication and characterization of PSCs

All the PSCs were prepared using the following fabrication procedure. Glass substrates (with a sheet resistance of 8Ω/sq.) coated with indium tin oxide (ITO) were patterned lithographically, cleaned with a detergent, ultrasonicated in acetone and isopropyl alcohol, dried on a hot plate at 120 °C for 5 min, and finally treated with oxygen plasma for 5 min. The hole-transporting material (PEDOT:PSS, Clevios P-VP AI4083) was passed through a 0.45 μm filter and then deposited on the ITO-coated glass substrate using the spin-coating method at a spinning rate 4000 rpm for 60 s. The thus-coated substrate was then placed on a hot plate and dried at 120 °C for 10 min. To form the photoactive layer in a binary PSC, a mixed solution of the fullerene derivative ($PC_{61}BM$ or $PC_{71}BM$) and copolymer (*r*-**PTTDPP50** or *r*-**PTTDPP75)** with a 1:2 wt ratio in *o*-DCB was stirred overnight and then filtered through a 0.2 μm poly(tetrafluoroethylene) filter. Further, to form the photoactive layer in a ternary PSC, *r*-**PTTDPP50**, P3HT, and $PC_{61}BM$ were mixed in various weight ratios in *o*-DCB. Subsequently, a photoactive layer consisting of the copolymer/fullerene derivative mixture was formed above the PEDOT:PSS layer by spin coating (600 rpm, 60 s) the mixture solution. The photoactive layer was then thermally treated at 140 °C for 10 min. A Ca-based (30 nm)/Al (100 nm) cathode was deposited thermally onto the photoactive thin film in a high-vacuum chamber; the active area of the deposited PSC was 4 mm^2. Following the deposition of the Al electrode, the PSCs were tested under ambient conditions. The photocurrent density-voltage (*J-V*) curves of the PSCs were obtained using a programmable electrometer with current and voltage sources (Keithley 2400) under 100 mW cm^{-2} solar light illumination from an AM 1.5G solar simulator (Oriel solar simulator). The illumination intensity was calibrated using a standard Si photodiode detector equipped with a KG-5 filter. In addition, the output photocurrent was adjusted to match the photocurrent of the Si reference cell, in order to obtain a power density of 100 mW cm^{-2}. To measure the incident photon-to-electron conversion efficiency (IPCE), a xenon lamp connected to a monochromator was used as the light source, and its output was monitored using a photodiode connected to a lock-in amplifier. All the electrical measurements were carried out in air.

3. Results and discussion

3.1. Characterization of copolymers

The processes for synthesizing *r*-**PTTDPP50** and *r*-**PTTDPP75** are shown in Scheme 1. **MTD** and **DPPBr** were synthesized according to previously reported procedures [36–39]. The two copolymers were obtained by the Stille cross-coupling reaction using **MTD**, **DPPBr**, and 2,5-bis(trimethylstannyl) thiophene in different feed-in ratios. The resulting copolymers were purified by repeated precipitation and Soxhlet extractions. *r*-**PTTDPP50** was soluble in various common organic solvents such as chloroform, THF, toluene, and *o*-DCB, while *r*-**PTTDPP75** showed limited solubility in these solvents. This limited solubility of *r*-**PTTDPP75** is probably attributable to the increase in the number of coplanar DPP units in the polymer main chains, as this increases the extent of π-stacking between the polymer chains. Table 1 presents the number-average (M_n) and weight-average (M_w) molecular weights of the polymers, as determined by GPC (THF was used as the eluent) with respect to polystyrene standards. The number-average molecular weights (M_n) of *r*-**PTTDPP50** and *r*-**PTTDPP75** were found to be 170.9 and 325.6 kg mol^{-1} respectively, while their polydispersity indices were 1.18 and 1.10, respectively.

The thermal stability of conjugated polymers is directly related on the operational stability of the optoelectronic devices. Therefore, the conjugated polymers used in PSCs should exhibit a high T_d (temperature at which a 5% weight loss occurred). As indicated in Table 1, *r*-**PTTDPP50** and *r*-**PTTDPP75** had T_d values of approximately 297 °C in an atmosphere of nitrogen. Thus, these copolymers exhibited a fairly high thermal stability, and hence, they are suitable for use in PSCs.

3.2. Optical properties of the conjugated copolymers

Fig. 1 shows the absorption spectra of *r*-**PTTDPP50** and *r*-**PTTDPP75** in toluene solutions and as thin films. Table 2 lists the absorption data of these copolymers. In the solution form, both copolymers exhibited a broad absorption spectrum with two obvious absorption peaks and an absorption edge for wavelengths higher than 1000 nm. The first absorption band, which was observed at 300–500 nm, originated from the n-π* transition of the conjugated side chain and the π-π* transition of the conjugated main chain. The second absorption band, seen at 500–1000 nm, was attributable to the intramolecular charge transfer interactions between the donors (thiophene-derivative units) and acceptors (diketopyrrolopyrrole units) along the main chain [16,40–42]. *r*-**PTTDPP75** exhibited broad absorption as well as a slight red-shift in the second absorption band at longer wavelengths, both in the solution form and thin-film state, when compared to *r*-**PTTDPP50**. This was attributable to the presence of a greater number of DPP units in its main chains, which resulted in an increase in the degree of effective conjugation of the polymer backbone. The absorption peaks of these copolymers in the thin-film state were red-shifted from those of the copolymers in solution form. Further, the absorption bands were also significantly broadened. These phenomena occurred because of π-π stacking interactions between the polymer chains. Generally, conjugated polymers with relatively broad absorption spectra are better suited for harvesting solar light. This characteristic of broad absorption is expected to improve the

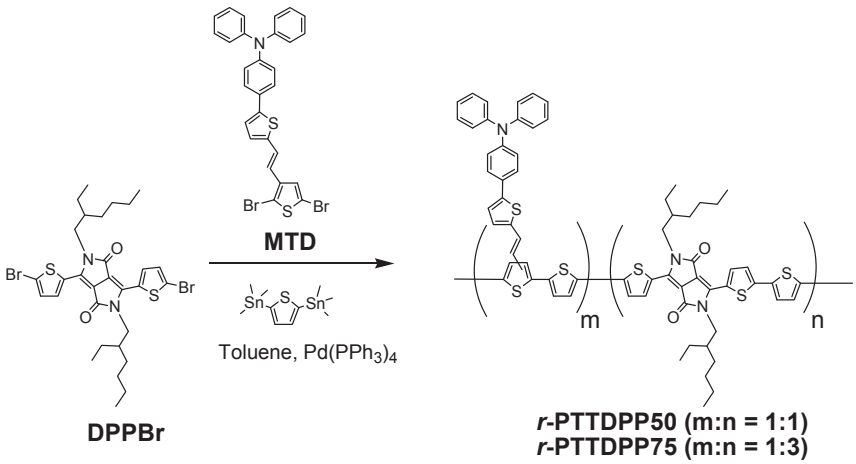

Scheme 1. Synthetic scheme for copolymers *r*-PTTDPP50 and *r*-PTTDPP75.

Table 1
Molecular weights and thermal properties of copolymers.

Copolymers	M_n[a] (kg/mol)	M_w[a] (kg/mol)	PDI (M_w/M_n)	T_d[b] (°C)
***r*-PTTDPP50**	170.9	203.2	1.18	297
***r*-PTTDPP75**	325.6	358.2	1.10	298

[a] M_n, M_w and PDI of the polymers were determined by GPC using polystyrene standards in THF.
[b] Temperature of 5% weight loss.

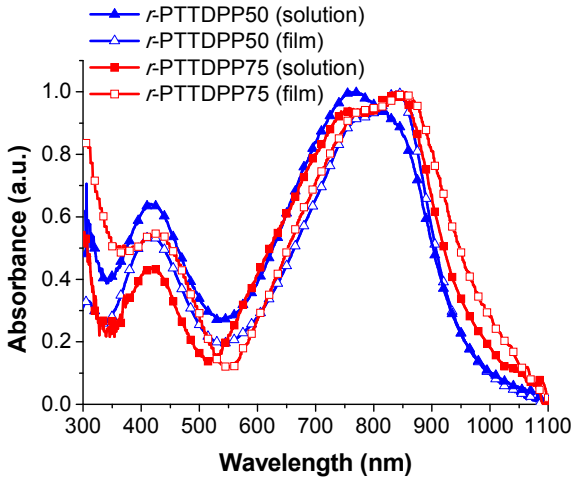

Fig. 1. UV–vis absorption spectra of copolymers in dilute toluene solutions and as thin films.

Table 2
Photophysical and electrochemical properties of copolymers.

Copolymers	In solution[a] (nm)	In film[b] (nm)	HOMO/LUMO[c] (eV)	E_g^{ec}[d] (V)
	λ_{max}^{abs}	λ_{max}^{abs}		
***r*-PTTDPP50**	413, 758	417, 842	–5.16/–3.89	1.27
***r*-PTTDPP75**	421, 843	428, 850	–5.19/–3.99	1.20

[a] Measured in toluene solution.
[b] Casted from *o*-DCB solution.
[c] The energy levels were calculated according to: HOMO $= -e(E_{on}^{ox} - E_{on}^{ferrocene} + 4.8)$(eV), LUMO $= -e\left(E_{on}^{red} - E_{on}^{ferrocene} + 4.8\right)$(eV).
[d] Estimated using empirical equations: $E_g^{ec} = E_{HOMO} - E_{LUMO}$.

absorption efficiency of the photoactive layer and hence increase the photocurrent induced in PSCs.

3.3. Electrochemical properties of conjugated copolymers

The electrochemical properties of the synthesized copolymers were elucidated by CV. The HOMO and LUMO energy levels of the conjugated copolymers were also estimated. Fig. 2 shows the oxidation and reduction behaviors of the copolymers, which were determined from their CV curves. The potentials were measured against a Ag/Ag^+ reference electrode while using a Pt counter electrode; a 0.1 M solution of tetrabutylammonium hexafluorophosphate in acetonitrile was used as the electrolyte. The scan rate was 100 mV S^{-1}. The HOMO values of ***r*-PTTDPP50** and ***r*-PTTDPP75** were calculated from the potentials at the onset of oxidation using the following equation (the HOMO level of ferrocene, which is 4.8 eV, was used as the reference):

$$\text{HOMO} = -e\left(E_{on}^{ox} - E_{on}^{reference} + 4.8\right)(\text{eV})$$

The HOMO levels of ***r*-PTTDPP50** and ***r*-PTTDPP75** were calculated to be −5.16 and −5.19 eV, respectively. Using the same method, the LUMO levels of ***r*-PTTDPP50** and ***r*-PTTDPP75** were estimated from the potentials at the onset of reduction using the

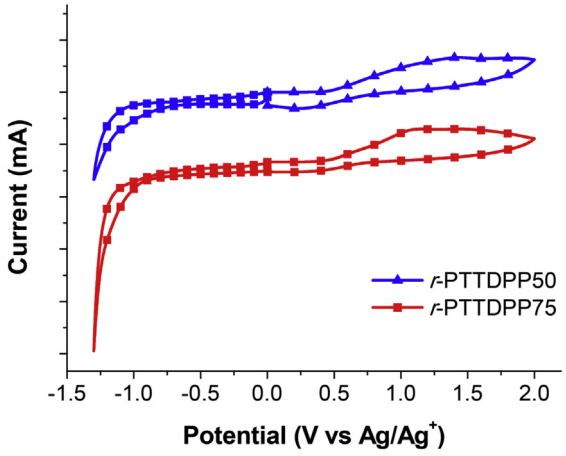

Fig. 2. Cyclic voltammograms of copolymer films on platinum plates in acetonitrile solution of 0.1 mol L^{-1} Bu_4NClO_4.

following equation:

$$\text{LUMO} = -e\left(E_{on}^{red} - E_{on}^{ferrocene} + 4.8\right)(eV)$$

The calculated LUMO levels of *r*-**PTTDPP50** and *r*-**PTTDPP75** were −3.89 and −3.99 eV, respectively. The electrochemical bandgap (E_g^{ec}) values were obtained by utilizing the differences between the HOMO and LUMO energy levels and were found to be 1.27 and 1.20 eV, respectively. Although the electrochemical bandgaps of these copolymers were almost identical, the LUMO level of *r*-**PTTDPP75** was slightly lower, because of the increase in the number of electron-accepting DPP moieties in the main chain. Table 2 presents the electrochemical properties of the copolymers.

3.4. PV properties of PSCs

The photovoltaic properties of the two copolymers were examined by fabricating PSCs using the copolymers as the donor and $PC_{61}BM$ or $PC_{71}BM$ as the acceptor. The fabricated devices had the following structure: ITO/PEDOT:PSS/copolymer:$PC_{61}BM$ or $PC_{71}BM$/Ca/Al. *o*-DCB was used to prepare the solution that was spin coated to fabricate the active layer; the concentration of the solution was 24 mg/mL. The optimal copolymer/$PC_{61}BM$ weight ratio for the ***r*-PTTDPP50**-based devices was found to be 1:2. Owing to the limited solubility of ***r*-PTTDPP75**, the weight ratio in the case of the ***r*-PTTDPP75**/$PC_{61}BM$-based device was also set to be 1:2, to allow for comparison. Fig. 3 plots the typical photocurrent density-voltage (*J*-*V*) characteristics of the PSCs prepared from copolymer/$PC_{61}BM$ and copolymer/$PC_{71}BM$, as measured under simulated AM 1.5 G illumination (100 mW/cm^2). Table 3 lists the PV properties of these PSCs, including their V_{oc}, short-circuit current density (J_{sc}), fill factor (FF), PCE values, series resistances (R_s) and shunt resistances (R_{sh}). The ***r*-PTTDPP50**/$PC_{61}BM$-based (w/w = 1:2) PSC exhibited a PCE of 1.36%, along with a J_{sc} of 5.12 mA/cm^2, a V_{oc} of 0.683 V, and an FF of 39.1%. In contrast, the ***r*-PTTDPP75**/$PC_{61}BM$-based (w/w = 1:2) PSC showed a lower PCE at 0.27%, along with a J_{sc} of 1.52 mA/cm^2, a V_{oc} of 0.502 V, and an FF of 35.5%. This is ascribed to the limited solubility of ***r*-PTTDPP75**, which results in phase separation in the blend film and limits further device optimization. Additionally, the ***r*-PTTDPP75**/$PC_{61}BM$-based PSC showed a V_{oc} of 0.502 V even though ***r*-PTTDPP75** has a lower HOMO level than that of ***r*-PTTDPP50**. Poor solubility of ***r*-PTTDPP75** hampered charge recombination at the donor/acceptor interface, leading to a decrease in V_{oc} [43,44]. The device efficiency could be further improved by using ***r*-PTTDPP50** and $PC_{71}BM$ (as the acceptor) in a 1:2 blending ratio. A higher photocurrent was normally obtained when $PC_{71}BM$ was used as an acceptor instead of $PC_{61}BM$ in the active layer; because $PC_{71}BM$ exhibits higher absorption in the visible region [42,45]. When $PC_{71}BM$ was used instead of $PC_{61}BM$ as the electron acceptor, the resulting ***r*-PTTDPP50**/$PC_{71}BM$-based (w/w = 1:2) device exhibited a higher J_{sc} value and a PCE of 1.92%. Numerous groups have recently demonstrated that device performance can be substantially enhanced through solvent treatments, which have been shown to modify the interface between PEDOT:PSS and the active layer or to prevent phase separation in BHJ cells [46–48]. To exploit this effect, the freshly spin-coated ***r*-PTTDPP50**/$PC_{71}BM$ (w/w = 1:2) blend film was treated with ethanol and subjected to a cathode evaporation process. The ethanol-treated ***r*-PTTDPP50**-based device exhibited a PCE of 2.32%, along with a J_{sc} of 9.81 mA/cm^2, a V_{oc} of 0.632 V, and an FF of 37.4%. Thus, the ethanol treatment led to a 21% enhancement in the PCE, with the V_{oc} and FF values also showing a slight increase over those of the untreated device. Finally, the J_{sc} value increased significantly. This phenomenon is ascribed to the fact that the ethanol treatment made the contact between the cathode and the active layer more compact, as evidenced by AFM measurements [49]. Ternary blend PSCs formed by using a blend of ***r*-PTTDPP50**:P3HT:$PC_{61}BM$ as the active layer were also fabricated, given the wide absorption range of ***r*-PTTDPP50** and the suitable energy alignment exhibited by P3HT and $PC_{61}BM$. The energy levels of the materials used in the ternary blend devices are illustrated in Fig. 4. To illustrate the effect of the proportion of ***r*-PTTDPP50** used on the performance of the resulting PSCs, the active layer with only P3HT and $PC_{61}BM$ was used as the reference. The structure of the ternary blend device was ITO/PEDOT:PSS/***r*-PTTDPP50**:P3HT:$PC_{61}BM$/Ca/Al, and the concentration of the solution used was 18 mg/mL. The donors-to-acceptor weight ratio was kept as 1:1, while the proportion of ***r*-PTTDPP50** in the donors was increased to 50 wt%. Fig. 5 shows the photocurrent density-voltage (*J*-*V*) characteristics of ***r*-PTTDPP50**:P3HT:$PC_{61}BM$ PSCs with 0 wt%, 10 wt%, 20 wt%, and 50 wt% ***r*-PTTDPP50**, as measured under simulated AM 1.5 G illumination (100 mW/cm^2). The PV characteristics of these PSCs are listed in Table 3. The proportion in which ***r*-PTTDPP50** was added strongly affected the device performance, including the V_{oc}, J_{sc}, FF, and PCE values. The V_{oc} and J_{sc} values increased initially when the ***r*-PTTDPP50** content was increased to 10 wt% and then decreased on further increasing the ***r*-PTTDPP50** content. The PSC with 10 wt% ***r*-PTTDPP50** showed an improved PCE (3.85%). Further, its J_{sc} increased from 7.91 to 9.36 mA/cm^2, V_{oc} increased from 0.605 to 0.637 V, and FF increased from 62.1% to 63.7%. The observed increase in the PCE corresponded to an improvement of 30% over that of the reference device. This was attributable to the wide absorption range of ***r*-PTTDPP50**, which increased the absorption in the long-wavelength region. Moreover, the energy levels of ***r*-PTTDPP50** form a bridge between those of P3HT and $PC_{61}BM$, facilitating charge transfer at the donor/acceptor interface. When the proportion of ***r*-PTTDPP50** was increased to 20 wt%, the V_{oc} and J_{sc} values decreased, while the FF value increased slightly. The decrease in J_{sc} is attributed to the disruption of the interpenetrating network between P3HT and $PC_{61}BM$ because of the increase in the amount of ***r*-PTTDPP50** present. However, the PCE of the device remained higher than that of the binary P3HT:$PC_{61}BM$ device. When a blend film with 50 wt% ***r*-PTTDPP50** was used, the V_{oc}, J_{sc}, and FF values decreased significantly. This was probably because of the lower degree of mixing of P3HT:$PC_{61}BM$ because of the presence of an excessive amount of ***r*-PTTDPP50**, resulting in a lack of percolation channels for charge transport. The FF value normally depends on the R_s and R_{sh} of PSCs, which are strongly coupled with exciton dissociation and charge carrier recombination in the active layer. The optimized exciton

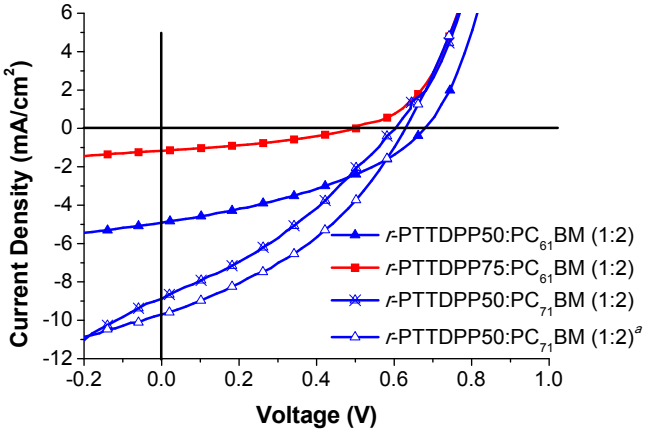

Fig. 3. *J*-*V* characteristics of bulk heterojunction solar cells fabricated from ***r*-PTTDPP50** and ***r*-PTTDPP75** under illumination of AM 1.5 G, 100 mW/cm^2.

Table 3
Photovoltaic performances of the bulk heterojunction solar cells.

active layer (w/w ratio)	V_{oc} (V)	J_{sc} (mA/cm^2)	FF (%)	PCE (%)	R_s (Ω cm^2)	R_{sh} (Ω cm^2)
r-PTTDPP50:$PC_{61}BM$ (1:2)	0.683	5.12	39.1	1.36	10.84	324
r-PTTDPP75:$PC_{61}BM$ (1:2)	0.502	1.52	35.5	0.27	11.53	625
r-PTTDPP50:$PC_{71}BM$ (1:2)	0.606	8.65	36.6	1.92	9.51	107
r-PTTDPP50:$PC_{71}BM$ (1:2)[a]	0.632	9.81	37.4	2.32	12.46	135
P3HT:$PC_{61}BM$ (1:1)	0.605	7.91	62.1	2.97	5.08	492
r-PTTDPP50:P3HT:$PC_{61}BM$ (0.1:0.9:1)	0.637	9.36	64.6	3.85	4.00	654
r-PTTDPP50:P3HT:$PC_{61}BM$ (0.2:0.8:1)	0.615	8.50	65.5	3.43	4.37	877
r-PTTDPP50:P3HT:$PC_{61}BM$ (0.5:0.5:1)	0.608	7.72	60.2	2.83	4.58	592

[a] Processed with ethanol.

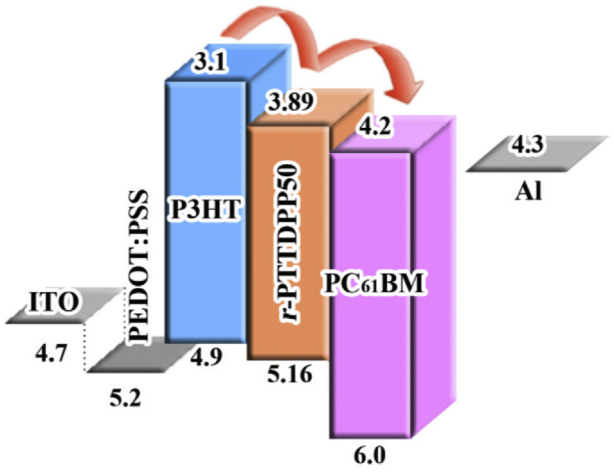

Fig. 4. Energy levels (eV) of electrodes and materials used in ternary blends.

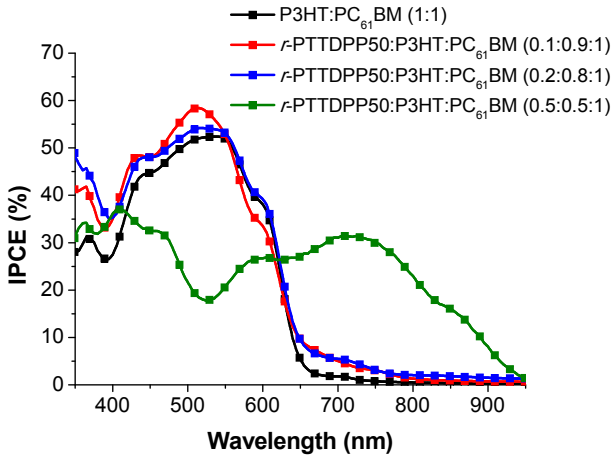

Fig. 6. EQE curves of P3HT:$PC_{61}BM$ (1:1) and ***r*-PTTDPP50**:P3HT:$PC_{61}BM$ devices with various ***r*-PTTDPP50** wt ratios.

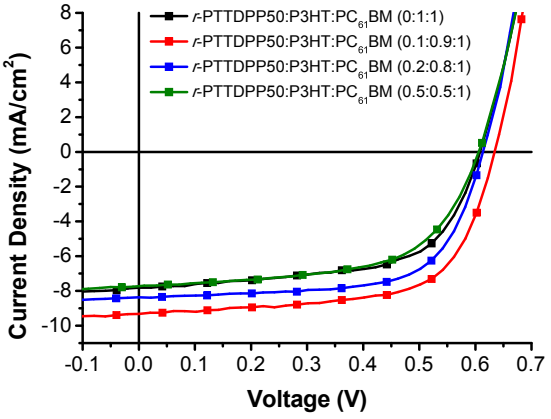

Fig. 5. *J-V* characteristics of bulk heterojunction solar cells with various ***r*-PTTDPP50** wt ratios under illumination of AM 1.5 G, 100 mW/cm^2.

dissociation and charge carrier transport suppress charge carrier recombination, thereby increasing the FF value [50]. As shown in Table 3, the blend film morphology of the binary PSCs seems to be more sensitive than the effect of device fabrication conditions (see Section 3.5 for a detailed discussion). For example, the ***r*-PTTDPP50**/$PC_{61}BM$-based (w/w = 1:2) binary PSC showed similar R_s but poor R_{sh} than that of ***r*-PTTDPP75**/$PC_{61}BM$-based (w/w = 1:2) binary PSC. Poor R_{sh} usually indicated more current leakage pathways due to charge recombination or trapping. However, ***r*-PTTDPP75**/$PC_{61}BM$-based (w/w = 1:2) binary PSC showed lower J_{sc} value than that of ***r*-PTTDPP50**. This implies that the poor performance of ***r*-PTTDPP75**/$PC_{61}BM$-based (w/w = 1:2) binary PSC is mainly owing to the limited solubility of ***r*-PTTDPP75**. As discussed above, poor solubility of ***r*-PTTDPP75** caused phase separation in the blend film and also hampered charge recombination at the donor/acceptor interface, leading to both decreases in V_{oc} and J_{sc}, as a result of poor device performance was obtained. In addition, the ethanol-treated ***r*-PTTDPP50**/$PC_{71}BM$-based (w/w = 1:2) binary PSC exhibited higher R_s and R_{sh} values than those of untreated device. The worse R_s and better R_{sh} complementary phenomena suggest that the slightly enhanced PCE and FF of the ethanol-treated device are ascribed to the improved nanomorphology of the blend film. For the ternary blend PSCs (also shown in Table 3), it was found that the FF values depend on R_s and R_{sh} when the ***r*-PTTDPP50** content was lower than 20 wt% (*r*-PTTDPP50:P3HT:$PC_{61}BM$ (0.1:0.9:1)-based and *r*-PTTDPP50:P3HT:$PC_{61}BM$ (0.2:0.8:1)-based devices). The R_s values were lower and the R_{sh} values were higher than those of the reference device which implied that the charge recombination or trapping was suppressed under suitable contents of ***r*-PTTDPP50**. When the proportion of ***r*-PTTDPP50** was increased to 50 wt% (*r*-PTTDPP50:P3HT:$PC_{61}BM$ (0.5:0.5:1)-based device), the R_s value increased but the R_{sh} value decreased; therefore, the FF decreased significantly. The external quantum efficiency (EQE) spectra of the P3HT:$PC_{61}BM$ (1:1 wt%) and ***r*-PTTDPP50**:P3HT:$PC_{61}BM$ ternary devices with various weight ratios were measured and are plotted in Fig. 6. The EQE profiles of the ternary PSCs containing up to 20 wt % ***r*-PTTDPP50** were similar, displaying a photocurrent response typical of P3HT:$PC_{61}BM$-based devices at 350–650 nm. Slight variations in the photocurrent response may be attributed to the differences in the active layer thickness or to optical interference within 100 nm of the active layers [51]. When ***r*-PTTDPP50** is added

to the P3HT:$PC_{61}BM$ blend film, the intensity of the photocurrent signal increased at 350–550 nm as well as in the NIR region, which suggested that the broader absorption region and higher EQE value contributed to the increase in the photocurrent generated. The increase in the J_{sc} value was thus attributable to the improved EQE and photovoltaic properties of the ternary blend device. When the concentration of ***r*-PTTDPP50** was increased to 50 wt%, the EQE in the P3HT absorption range decreases, while that in the NIR region increases significantly. However, a substantial drop in the EQE in the entire region was also observed.

3.5. AFM imaging

In order to further elucidate the relationship between film morphology and device performance, tapping-mode AFM was employed to characterize the morphologies of the active layers. Fig. 7 shows the AFM images of blend films identical to the active layers used in the devices listed in Table 3. Fig. 7(a)–(d) display the morphologies of the ***r*-PTTDPP50**/$PC_{61}BM$, ***r*-PTTDPP75**/$PC_{61}BM$, ***r*-PTTDPP50**/$PC_{71}BM$, and ethanol-treated ***r*-PTTDPP50**/$PC_{71}BM$ binary blend films. The thin film of the ***r*-PTTDPP50**/$PC_{61}BM$ blend (Fig. 7(a)) with a 1:2 wt ratio had a smooth surface (root-mean-square (RMS) roughness = 0.28 nm), implying that this blend film exhibited satisfactory miscibility. However, as can be seen in Fig. 7(b), the ***r*-PTTDPP75**/$PC_{61}BM$ blend film with a 1:2 wt ratio exhibited clear agglomerates, with its RMS roughness being 0.60 nm, indicating that the device performance was strongly affected by the morphology of the blend film used. This is ascribed to the limited solubility of ***r*-PTTDPP75**, which resulted in the large-scale phase separation of ***r*-PTTDPP75** and $PC_{61}BM$. As a result, the J_{sc} value of the ***r*-PTTDPP75**/$PC_{61}BM$-based device was markedly low. When the acceptor $PC_{61}BM$ was replaced with $PC_{71}BM$, as shown in Fig. 7(c), the resulting ***r*-PTTDPP50**/$PC_{71}BM$ (w/w = 1:2) blend film exhibited a smoother surface and a homogeneous dispersion (RMS roughness = 0.23 nm) than did the ***r*-PTTDPP50**/$PC_{61}BM$ blend film. Thus, a suitable domain size and the prevention of phase separation optimize the photovoltaic performance. Moreover, a higher photocurrent is usually obtained by replacing $PC_{61}BM$ with $PC_{71}BM$ as the acceptor in the active layer [45]. As expected, both J_{sc} and PCE were higher for the ***r*-PTTDPP50**/$PC_{71}BM$-based (w/w = 1:2) PSC than the $PC_{61}BM$-containing device. To elucidate the effect of ethanol treatment, the morphologies of the treated films were also examined, as shown in Fig. 7(d). When a small amount of ethanol was added to the ***r*-PTTDPP50**/$PC_{71}BM$ (w/w = 1:2) blend, the surface roughness (RMS roughness = 0.24 nm) of the active layer was similar to that of the blend film without ethanol. However, the $PC_{71}BM$ particles could be seen more clearly on the surface of the blend film with ethanol. This suggests that the improvement in the PCE of the PSCs after the ethanol treatment was owing to a better contact between $PC_{71}BM$ and the cathode. Fig. 7(e)–(h) show the morphologies of the P3HT:$PC_{61}BM$, ***r*-PTTDPP50**$_{0.1}$:$P3HT_{0.9}$:$PC_{61}BM_1$, ***r*-PTTDPP50**$_{0.2}$:$P3HT_{0.8}$:$PC_{61}BM_1$, and ***r*-PTTDPP50**$_{0.5}$:$P3HT_{0.5}$:$PC_{61}BM_1$ ternary blend films and their corresponding RMS roughness values, which were 0.65, 0.72, 0.65, and 0.64 nm, respectively. When the proportion of ***r*-PTTDPP50** was 10 wt%, small phase-separation domains were observed, and the film surface was relatively coarse. These domains are most likely the percolation channels that form between the two polymers and facilitate charge transport, leading to an increase in J_{sc} [52]. This is in agreement with the observed *J-V* characteristics and EQE value. The small phase-separation domains became more obvious with an increase in the proportion of ***r*-PTTDPP50** added. Large domains suppress the crystallinity of P3HT and thus cause a decrease in device performance. It should be noted that the PCE of the ternary PSCs was high when the proportion of ***r*-PTTDPP50** was lower than 20 wt%.

4. Conclusions

In conclusion, two new two-dimensional conjugated copolymers (named *r*-**PTTDPP50** and *r*-**PTTDPP75)** consisting of a DPP derivative, thiophene with conjugated side chains, and 2,5-bis(trimethylstannyl)thiophene were successfully designed and synthesized via Stille cross-coupling reactions for use in BHJ PSCs; the copolymers were obtained by varying the feed-in ratios. In the thin-film form, both the synthesized copolymers exhibited broad absorption spectra as well as an absorption edge for wavelengths

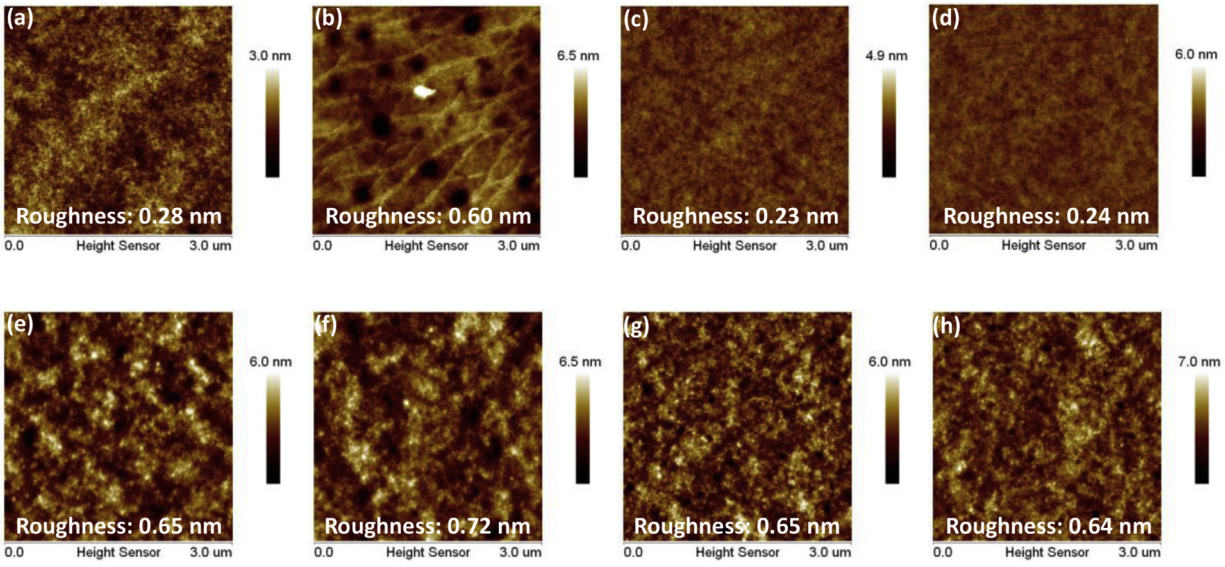

Fig. 7. AFM topographic images of (a) ***r*-PTTDPP50**:$PC_{61}BM$ (1:2), (b) ***r*-PTTDPP75**:$PC_{61}BM$ (1:2), (c) ***r*-PTTDPP50**:$PC_{71}BM$ (1:2), (d) Ethanol-treated ***r*-PTTDPP50**:$PC_{71}BM$ (1:2), (e) P3HT:$PC_{61}BM$ (1:1), (f) ***r*-PTTDPP50**:P3HT:$PC_{61}BM$ (0.1:0.9:1), (g) ***r*-PTTDPP50**:P3HT:$PC_{61}BM$ (0.2:0.8:1), and (h) ***r*-PTTDPP50**:P3HT:$PC_{61}BM$ (0.5:0.5:1), in tapping mode. Area of all images is 300 nm × 300 nm.

greater than 1000 nm. On increasing the number of coplanar and electron-withdrawing DPP units in the main chain, a broad absorption spectrum and a relative low LUMO energy level were obtained. For the BHJ PSC devices based on *r*-**PTTDPP50** and *r*-**PTTDPP75** and $PC_{61}BM$ or $PC_{71}BM$, the PCE values were 0.27%–2.32%. More importantly, ternary blend PSCs were also fabricated, given the wide absorption range of ***r*-PTTDPP50** and the suitable energy alignment between P3HT and $PC_{61}BM$. The device based on the ***r*-PTTDPP50**:P3HT:$PC_{61}BM$ (0.1:0.9:1 wt%) blend film had the highest PCE (3.85%) and a J_{sc} of 9.36 mA/cm^2, a V_{oc} of 0.637 V, and an FF of 64.6%; this was a 30% improvement over the P3HT:$PC_{61}BM$ binary blend-based device. The best ternary blend device showed an improved light harvesting ability and better morphology, as evidenced by its EQE spectrum and AFM images. This work provides a feasible synthesis route to construct a series of 2D low-bandgap materials with broad absorptions by varying the feed-in ratios of the monomers. Further, these materials can also be used as second sensitizers in ternary blend systems to fabricate efficient PSCs.

Acknowledgments

The financial support provided by the Ministry of Science and Technology, Taiwan (ROC), under contract no. MOST 103-2113-M-260-005 and MOST 104-2113-M-260-001, is gratefully acknowledged.

References

[1] J. Halls, C. Walsh, N. Greenham, E. Marseglia, R. Friend, S. Moratti, A. Holmes, Nature 376 (1995) 498–500.
[2] G. Yu, J. Gao, J. Hummelen, F. Wudl, A. Heeger, Science 270 (1995) 1789–1790.
[3] C.J. Brabec, S. Gowrisanker, J.J.M. Halls, D. Laird, S. Jia, S.P. Williams, Adv. Mater. 22 (2010) 3839–3856.
[4] Z. He, C. Zhong, S. Su, M. Xu, H. Wu, Y. Cao, Nat. Photonics 6 (2012) 591–595.
[5] X. Guo, M. Zhang, W. Ma, L. Ye, S. Zhang, S. Liu, H. Ade, F. Huang, J. Hou, Adv. Mater. 26 (2014) 4043–4049.
[6] J. You, L. Dou, K. Yoshimura, T. Kato, K. Ohya, T. Moriarty, K. Emery, C.-C. Chen, J. Gao, G. Li, Y. Yang, Nat. Commun. 4 (2013) 1446.
[7] T.M. Clarke, J.R. Durrant, Chem. Rev. 110 (2010) 6736–6767.
[8] A.J. Heeger, Adv. Mater. 26 (2014) 10–28.
[9] Y. Li, Acc. Chem. Res. 45 (2012) 723–733.
[10] A.W. Hains, Z. Liang, M.A. Woodhouse, B.A. Gregg, Chem. Rev. 110 (2010) 6689–6735.
[11] K. Vandewal, K. Tvingstedt, A. Gadisa, O. Inganas, J.V. Manca, Nat. Mater. 8 (2009) 904–909.
[12] J.I. Basham, G.K. Mor, C.A. Grimes, ACS Nano 4 (2010) 1253–1258.
[13] L. Dou, J. You, J. Yang, C.-C. Chen, Y. He, S. Murase, T. Moriarty, K. Emery, G. Li, Y. Yang, Nat. Photonics 6 (2012) 180–185.
[14] C.-C. Chen, L. Dou, R. Zhu, C.-H. Chung, T.-B. Song, Y.B. Zheng, S. Hawks, G. Li, P.S. Weiss, Y. Yang, ACS Nano 6 (2012) 7185–7190.
[15] J.C. Bijleveld, A.P. Zoombelt, S.G.J. Mathijssen, M.M. Wienk, M. Turbiez, D.M. de Leeuw, R.A.J. Janssen, J. Am. Chem. Soc. 131 (2009) 16616–16617.
[16] P.P. Khlyabich, B. Burkhart, C.F. Ng, B.C. Thompson, Macromolecules 44 (2011) 5079–5084.
[17] J.S. Ha, K.H. Kim, D.H. Choi, J. Am. Chem. Soc. 133 (2011) 10364–10367.
[18] J.S. Lee, S.K. Son, S. Song, H. Kim, D.R. Lee, K. Kim, M.J. Ko, D.H. Choi, B. Kim, J.H. Cho, Chem. Mater. 24 (2012) 1316–1323.
[19] J. Yuan, X. Huang, F. Zhang, J. Lu, Z. Zhai, C. Di, Z. Jiang, W. Ma, J. Mater. Chem. 22 (2012) 22734–22742.
[20] K.H. Hendrik, G.H.L. Heintges, V.S. Gevaerts, M.M. Wienk, R.A.J. Janssen, Angew. Chem. Int. Ed. 52 (2013) 8341–8344.
[21] S. Zhang, L. Ye, Q. Wang, Z. Li, X. Guo, L. Huo, H. Fan, J. Hou, J. Phys. Chem. C 117 (2013) 9550–9557.
[22] Y. Li, C.-Y. Chang, Y. Chen, Y. Song, C.-Z. Li, H.-L. Yip, A.K.-Y. Jen, C. Li, J. Mater. Chem. C 1 (2013) 7526–7533.
[23] T.I. Ryu, Y. Yoon, J.-H. Kim, D.-H. Hwang, M.J. Ko, D.-K. Lee, J.Y. Kim, H. Kim, N.-G. Park, B. Kim, H.J. Son, Macromolecules 47 (2014) 6270–6280.
[24] Y. Li, Y. Zou, Adv. Mater. 20 (2008) 2952–2958.
[25] L. Huo, S. Zhang, X. Guo, F. Xu, Y. Li, J. Hou, Angew. Chem. Int. Ed. 50 (2011) 9697–9702.
[26] M. Wang, X. Hu, P. Liu, W. Li, X. Gong, F. Huang, Y. Cao, J. Am. Chem. Soc. 133 (2011) 9638–9641.
[27] H. Zhou, L. Yang, A.C. Stuart, S.C. Price, S. Liu, W. You, Angew. Chem. Int. Ed. 50 (2011) 2995–2998.
[28] F. Huang, K.S. Chen, H.L. Yip, S.K. Hau, O. Acton, Y. Zhang, J.D. Luo, A.K.-Y. Jen, J. Am. Chem. Soc. 131 (2009) 13886–13887.
[29] Z. Gu, P. Tang, B. Zhao, H. Luo, X. Guo, H. Chen, G. Yu, X. Liu, P. Shen, S. Tan, Macromolecules 45 (2012) 2359–2366.
[30] X. Guo, M.J. Zhang, J.H. Tan, S.Q. Zhang, L.J. Huo, W.P. Hu, Y.F. Li, J.H. Hou, Adv. Mater. 24 (2012) 6536–6541.
[31] M. Koppe, H.-J. Egelhaaf, E. Clodic, M. Morana, L. Lüer, A. Troeger, V. Sgobba, D.M. Guldi, T. Ameri, C.J. Brabec, Adv. Energy Mater. 3 (2013) 949–958.
[32] T. Ameri, P. Khoram, J. Min, C.J. Brabec, Adv. Mater. 25 (2013) 4245–4266.
[33] T. Ameri, J. Min, N. Li, F. Machui, D. Baran, M. Forster, K.J. Schottler, D. Dolfen, U. Scherf, C.J. Brabec, Adv. Energy Mater. 2 (2012) 1198–1202.
[34] Z. Hu, S. Tang, A. Ahlvers, S.I. Khondaker, A.J. Gesquiere, Appl. Phys. Lett. 101 (2012) 053308–053312.
[35] Q. An, F. Zhang, L. Li, J. Wang, J. Zhang, L. Zhou, W. Tang, ACS Appl. Mater. Interfaces 6 (2014) 6537–6544.
[36] L. Huo, J. Huo, H.-Y. Chen, S. Zhang, Y. Jiang, T.L. Chen, Y. Yang, Macromolecules 42 (2009) 6564–6571.
[37] H.-J. Wang, L.-H. Chan, C.-P. Chen, S.-L. Lin, R.-H. Lee, R.-J. Jeng, Polymer 52 (2011) 326–338.
[38] H.-J. Wang, L.-H. Chan, C.-P. Chen, R-H. Lee, W.-C. Su, R.-J. Jeng, Thin Solid Films 519 (2011) 264–5269.
[39] Y.-R. Liu, L.-H. Chan, H.-Y. Tang, J. Polym. Sci. Part A Polym. Chem. 53 (2015) 2878–2889.
[40] Y. Zhu, R.D. Champion, S.A. Jenekhe, Macromolecules 39 (2006) 8712–8719.
[41] P.M. Beaujuge, C.M. Amb, J.R. Reynolds, Acc. Chem. Res. 43 (2010) 1396–1407.
[42] L.-H. Chan, L.-C. Lin, C.-H. Yao, Y.-R. Liu, Z.-J. Jiang, T.-Y. Cho, Thin Solid Films 544 (2013) 386–391.
[43] Y. Wang, X. Xin, Y. Lu, T. Xiao, N. Zhao, X. Hu, B.S. Ong, S.C. Ng, Macromolecules 46 (2013) 9587–9592.
[44] Q. Fan, Y. Liu, P. Yang, W. Su, M. Xiao, J. Chen, M. Li, X. Wang, Y. Fang, H. Tan, R. Yang, W. Zhu, Org. Electron. 23 (2015) 124–132.
[45] Y. Liang, Y. Wu, D. Feng, S.T. Tsai, H.J. Son, G. Li, L. Yu, J. Am. Chem. Soc. 131 (2009) 56–57.
[46] D. Alemu, H.-Y. Wei, K.-C. Ho, C.-W. Chu, Energy Environ. Sci. 5 (2012) 9662–9671.
[47] H. Zhou, Y. Zhang, J. Seifter, S.D. Collins, C. Luo, G.C. Bazan, T.-Q. Nguyen, A.J. Heeger, Adv. Mater. 25 (2013) 1646–1652.
[48] J. Yu, Y. Zheng, J. Huang, Polymers 6 (2014) 2473–2509.
[49] X. Zhu, F. Zhang, Q. An, H. Huang, Q. Sun, L. Li, F. Teng, W. Tang, Sol. Energy Mater. Sol. Cells 132 (2015) 528–534.
[50] Q. An, F. Zhang, L. Li, J. Wang, Q. Sun, J. Zhang, W. Tang, Z. Deng, ACS Appl. Mater. Interfaces 7 (2015) 3691–3698.
[51] T. Ameri, P. Khoram, T. Heumüller, D. Baran, F. Machui, A. Troeger, V. Sgobba, D.M. Guldi, M. Halik, S. Rathgeber, U. Scherf, C.J. Brabec, J. Mater. Chem. A 2 (2014) 19461–19472.
[52] M.C. Chen, D.J. Liaw, Y.C. Huand, H.Y. Wu, Y. Tai, Sol. Energy Mater. Sol. Cells 95 (2011) 2621–2627.